Check for updates

ARTICLE

QSER1 preserves the suppressive status of the pro-apoptotic genes to prevent apoptosis

Xiru Zhao[1,8], Ke Fang[1,8], Xiaoxu Liu[1,8], Ruihuan Yao[1], Min Wang[1], Fanfan Li[1], Shaohua Hao[1], Jingjing He[1], Yan Wang[1], Menghan Fan[1], Wei Huang[2], Yiping Li[3], Chun Gao[4], Chengqi Lin [1,5,6✉] and Zhuojuan Luo [1,5,7✉]

Activation of the pro-apoptotic genes by the p53 family is a critical step in induction of apoptosis. However, the molecular signaling underlying their suppression remains largely unknown. Here, we report a general role of QSER1 in preventing apoptosis. QSER1 is widely up-regulated in multiple cancers, and its up-regulation correlates with poor clinic outcomes. QSER1 knockdown significantly promotes apoptosis in both p53 wild type and mutant cancer cells. Interestingly, we show that QSER1 and p53 occupy distinct cis-regulatory regions in a common subset of the pro-apoptotic genes, and function antagonistically to maintain their proper expression. Furthermore, we identify a key regulatory DNA element named QSER1 binding site in PUMA (QBP). Deletion of QBP de-represses PUMA and induces apoptosis. Mechanistically, QSER1 functions together with SIN3A to suppress PUMA in a p53-dependent and -independent manner, suggesting that QSER1 inhibition might be a potential therapeutic strategy to induce apoptosis in cancers.

INTRODUCTION

Apoptosis is a critical intracellular mechanism to maintain developmental balance and tissue homeostasis in multicellular organisms [1]. The impaired ability to undergo apoptosis leads to carcinogenesis, and promotes cancer progression and metastasis [2]. As a tumor suppressor, one of the major functions of p53 is induction of apoptosis through its transactivation activity towards the genes in the apoptotic pathways [3]. p53 is activated and stabilized in response to genotoxic insults, in turn, binds and activates the p53 response element (p53-RE) containing promoters of its downstream genes, such as *PUMA/BBC3* and *BAX* in the pro-apoptotic BCL-2 family [4].

Provoking apoptosis through p53 activation represents a promising strategy in cancer therapy [5]. However, *TP53*, the gene encoding p53, is among the most frequently mutated genes in various human cancers. More than half of human tumors carry mutations in *TP53*. Almost 80% of the cancer-derived p53 mutants lose the ability to bind DNA [6]. Most of the p53 downstream pro-apoptotic genes are usually maintained at very low levels, and hardly induced in p53 heavily damaged cancers. For example, PUMA (encoded by the *BBC3* gene) is a potent apoptosis mediator and accounts for the majority of the apoptotic activity of p53 [7]. It binds the anti-apoptotic BCL-2 family proteins to trigger mitochondrial outer membrane permeabilization (MOMP) and

apoptosis [8]. PUMA is barely detected in many types of human cancers [9]. Deficiency in PUMA activation increases cancer risk and suppresses antitumor effects of chemotherapeutic agents, as a consequence of apoptosis failure [10]. It is therefore critical to understand general mechanisms underlying how the p53 target transcriptional program can be suppressed in both p53 wild type (WT) and p53 deficient cancers.

The *QSER1* gene is located on band p13 of human chromosome 11, which is among the most frequently altered chromosomes in cancers [11–13]. Genome-wide association studies (GWAS) identified a SNP near *QSER1* associated with older onset age of Parkinson's disease [14]. Exome sequencing revealed that QSER1 could be a potential marker of type 2 diabetes [15]. In addition, it has been reported that the plasma QSER1 peptide levels are highly elevated in ovarian cancer patients [16]. Furthermore, a recent study has shown that QSER1 cooperates with TET1 to maintain low methylation status at the DNA methylation valleys [17]. We recently reported that QSER1 physically interacts with the Kruppel-like transcription factor ZFP281, a key regulator in embryonic stem cells, and locates at the bivalent regions [18–21]. However, the expression and function of QSER1 in cancers remain largely unknown.

Here we find that QSER1 is generally up-regulated in multiple cancers, and its up-regulation is strongly associated with poor

[1]Key Laboratory of Developmental Genes and Human Disease, School of Life Science and Technology, Southeast University, Nanjing 210096, China. [2]Jiangsu Provincial Key Laboratory of Critical Care Medicine, Department of Critical Care Medicine, Zhongda Hospital, School of Medicine, Southeast University, Nanjing 210009, China. [3]Department of Pathology, School of Medicine, Southeast University, Nanjing 210009, China. [4]Department of Gastroenterology, China-Japan Friendship Hospital, Beijing 100029, China. [5]Shenzhen Research Institute, Southeast University, 19 Gaoxin South 4th Road, Nanshan District, Shenzhen 518063, China. [6]Jiangsu Province Hi-Tech Key Laboratory for Biomedical Research, School of Life Science and Technology, Southeast University, Nanjing 210096, China. [7]Jiangsu Provincial Key Laboratory of Critical Care Medicine, School of Life Science and Technology, Southeast University, Nanjing 210096, China. [8]These authors contributed equally: Xiru Zhao, Ke Fang, Xiaoxu Liu. ✉email: cqlin@seu.edu.cn; zjluo@seu.edu.cn
Edited by K. Newton

clinic outcomes of different cancers. QSER1 knockdown significantly inhibits cell growth, colony formation, and up-regulates the p53 target pro-apoptotic genes, leading to apoptosis in both p53 WT and deficient cancer cells. Genome-wide occupancy analyses demonstrate that QSER1 occupies many of the p53 target genes, and suppresses their expression. Further studies reveal that QSER1 functions together with SIN3A in a p53-dependent and -independent manner to suppress *PUMA*. In summary, our studies indicate that QSER1 is a generic anti-apoptosis factor functioning in suppressing the pro-apoptotic genes, irrespective of p53 status.

RESULTS
Elevated QSER1 expression is associated with poor clinical outcomes in cancers
Recent large-scale studies highlighted the association of QSER1 with multiple diseases including cancers [14–16]. To explore the potential roles of QSER1 in cancer, we first analyzed QSER1 expression in human cancers using the Cancer Genome Atlas (TCGA) dataset [22]. 10 out of 18 examined cancers showed up-regulated QSER1 expression, compared with normal tissues ($P < 0.001$) in the database (Fig. 1A). Consistently, the immunohistochemistry (IHC) staining in pancreatic and bowel cancer patient samples confirmed the increased QSER1 expression in cancer tissues (Figs. 1B, S1A). The protein levels of QSER1 were also analyzed in a tissue microarray (TMA) cohort by IHC analysis, which included 49 pancreatic cancer samples with normal adjacent tissues as controls. The optimal cut-off value of QSER1 expression was determined by the receiver operating characteristic (ROC) analysis (Fig. S1B). The results indicated that QSER1 was overexpressed in 83.67% of the pancreatic cancer samples (Fig. 1C, D).

We next investigated the association of QSER1 expression levels with cancer prognosis. Kaplan–Meier (KM) plots analysis revealed that high levels of QSER1 were associated with poor clinical outcomes in various types of cancers, including pheochromocytoma and paraganglioma, pancreatic cancer, liver hepatocellular carcinoma, stomach adenocarcinoma and sarcoma (Fig. 1E). We examined the mutation status of *QSER1* in the pan-cancer mutation database, and found that mutations of *QSER1* in cancers include amplification, missense, truncating, gene fusion (Fig. 1F). *QSER1* copy-number was positively correlated with the RNA levels of QSER1 (Fig. 1F), suggesting that *QSER1* amplification might lead to its overexpression in cancers. Taken together, our data demonstrate that QSER1 is highly up-regulated in multiple cancers, and that its up-regulation is associated with poor prognosis.

QSER1 knockdown induces apoptosis in cancer cells
Given the poor clinical outcome in QSER1 highly expressed cancers, we examined the levels of QSER1 in response to the anti-cancer chemotherapy drug 5-FU in HCT116 cells. The apoptosis indicator cleaved-caspase 3 can be effectively induced in cells treated with the anti-cancer agent. Interestingly, QSER1 was significantly down-regulated when the cells underwent apoptosis after 5-FU treatment (Fig. 2A). To exclude the possibility that QSER1 is downregulated as a consequence of apoptosis, we used the pan-caspase inhibitor Z-VAD-FMK to treat the cells, and found that addition of Z-VAD-FMK inhibited the 5-FU induced apoptosis, as cleaved-caspase3 was undetectable in the cells co-treated with Z-VAD-FMK and 5-FU. Despite inhibiting apoptosis, Z-VAD-FMK treatment was not able to restore the levels of QSER1 in the 5-FU exposed cells (Fig. S2A).

To further investigate whether QSER1 could promote cancer progression, we depleted QSER1 in various cancer cell lines. Quantitative reverse transcription PCR (RT-qPCR) analyses demonstrated that QSER1 was effectively depleted in colon cancer cell HCT116, lung cancer cell A549, and stomach cancer cell SNU216 with two independent shRNAs (Fig. S2B). CCK-8 assays indicated

that QSER1 knockdown inhibited cancer cell proliferation (Fig. 2B). In addition, QSER1 knockdown significantly impaired cancer cell clonogenicities (Fig. 2C, D), and led to substantial increases in G1 cell fraction (Fig. S2C). Next, we tested whether the impaired cell viability after QSER1 knockdown was due to apoptosis. Annexin V-FITC and PI staining followed by FACS analyses revealed that, indeed, QSER1 depletion was able to induce apoptosis in HCT116, A549, and SNU216 cells (Fig. 2E). Western blot confirmed the substantial up-regulation of cleaved-caspase 3 after QSER1 depletion in multiple cancer cell lines including the above three cells (Figs. 2F–H, S2D). In addition, we employed the CRISPR-Cas9 technique to deplete QSER1 in HCT116 cell by using two independent sgRNAs (Fig. S2E), and found that CRISPR-Cas9 mediated QSER1 depletion also resulted in increased cleaved caspase 3 levels and apoptotic cell percentages (Fig. S2F, G), further substantiating a potent role of QSER1 in suppressing apoptosis.

QSER1 represses the p53 target pro-apoptotic genes
To dissect how QSER1 functions in anti-apoptosis, we conducted RNA sequencing (RNA-seq) analyses in control and QSER1 depleted HCT116 cells (Fig. S3A, B), and identified 810 differentially expressed genes (DEGs), of which 362 and 448 were commonly upregulated and downregulated by the two different QSER1 shRNAs (Fig. S3C). Gene ontology (GO) analysis revealed that the QSER1-regulated genes were significantly enriched in the processes of cell cycle, p53 signaling pathway, and negative regulation of growth (Fig. S3D). KEGG pathway analysis also identified p53 signaling pathway as the most affected pathway after QSER1 knockdown (Fig. 3A). Indeed, QSER1 depletion led to upregulation of many known p53 direct target genes (Fig. 3B). For examples, *BAX*, *PUMA/PUMA*, *CDKN1A/p21* and *CDK6* were de-repressed after QSER1 depletion (Fig. 3B). Given the activating roles of p53 on these genes, our results suggest that QSER1 might act in the opposite direction of p53 to suppress their expression.

p53 signaling pathway is involved in multiple biological processes, including DNA damage repair, cell cycle arrest, apoptosis, and aging [23, 24]. Network analysis by Metascape suggested that the QSER1-regulated genes were highly connected and clustered, and that the genes in p53 signaling pathway regulated by QSER1 were mostly involved in cell cycle and cell death (Figs. 3C, S3E). RT-qPCR validated the upregulation of the pro-apoptotic genes *PUMA* and *BAX* after QSER1 depletion in HCT116, A549, the lung cancer cell H1299, and the pancreatic cancer cell PANC-1 (Figs. 3D, S3F). In contrast, QSER1-mediated repression of the cell cycle gene *p21* only occurred in HCT116 and A549 cells, but not the rest of the tested cell lines (Fig. 3D). These results imply that QSER1 may have a general role in repressing the p53 target pro-apoptotic genes and thus regulate cancer progression.

QSER1 and p53 occupy distinct regulatory elements of the same subset of pro-apoptotic genes
IHC and immunofluorescence analyses revealed that QSER1 was predominantly localized in nuclei (Figs. 1B, 3E). To further explore whether and how QSER1 directly regulates the expression of pro-apoptotic genes, we carried out QSER1 ChIP-seq in HCT116 and A549 cells, and identified 3,669 and 5,274 significant QSER1 peaks in the two cell lines, respectively. QSER1 was mainly detected in the transcription start site (TSS) regions co-occupied by RNA polymerase II and the active gene mark H3K4me3; while less than 30% of the QSER1 peaks were located in intragenic or intergenic regions (Figs. 3F, G, S4A, B). KEGG pathway analysis displayed that QSER1-associated genes were significantly enriched in multiple cancer-related pathways in both HCT116 and A549 cells (Fig. S4C, D).

We further combined genomic occupancy profiles with the RNA-seq data to identify QSER1 direct target genes in HCT116 cells. 175 of the 810 DEGs after QSER1 knockdown were also
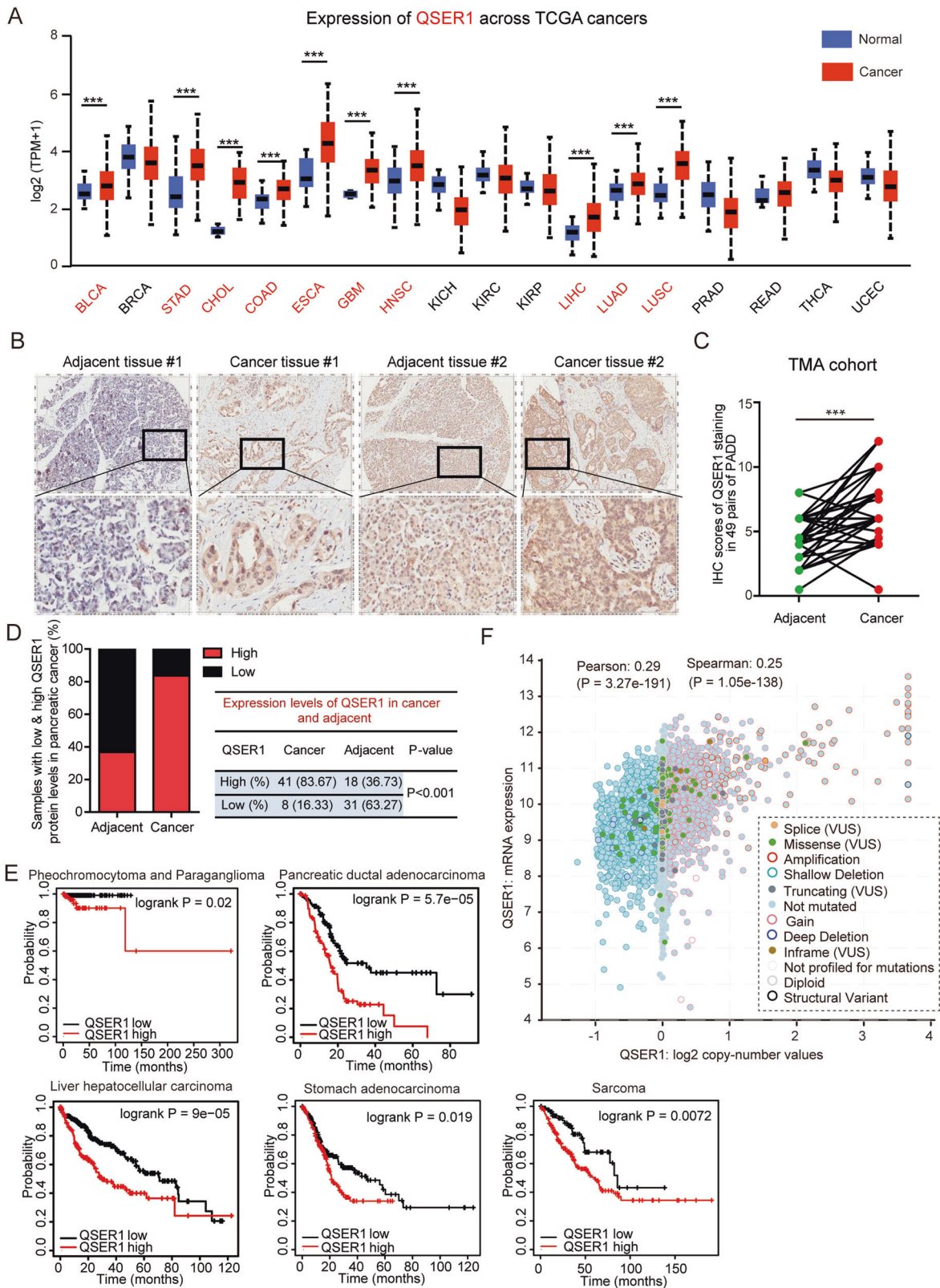
Fig. 1 Elevated QSER1 expression in multiple cancers is associated with poor clinical outcomes. A Expression of QSER1 across TCGA cancers. ***P < 0.001. **B** Representative images showing QSER1 expression in pancreatic cancer and matched adjacent tissues. **C** Paired analyses showing QSER1 IHC scores in the pancreatic cancer TMA cohort with both cancer and adjacent tissues. ***P < 0.001. **D** Samples in the pancreatic cancer TMA cohort with both cancer and adjacent tissues were classified based on the QSER1 protein levels. **E** Kaplan-Meier (KM) plots showing the overall survival of patients with pheochromocytoma and paraganglioma, liver hepatocellular carcinoma, pancreatic ductal adenocarcinoma, sarcoma, or stomach adenocarcinoma stratified by QSER1 expression level. The five types of cancers were chosen from the Kaplan–Meier plotter database according to the criteria of P value < 0.05. **F** The mutation types of QSER1 and the correlation of QSER1 copy number and mRNA expression level.
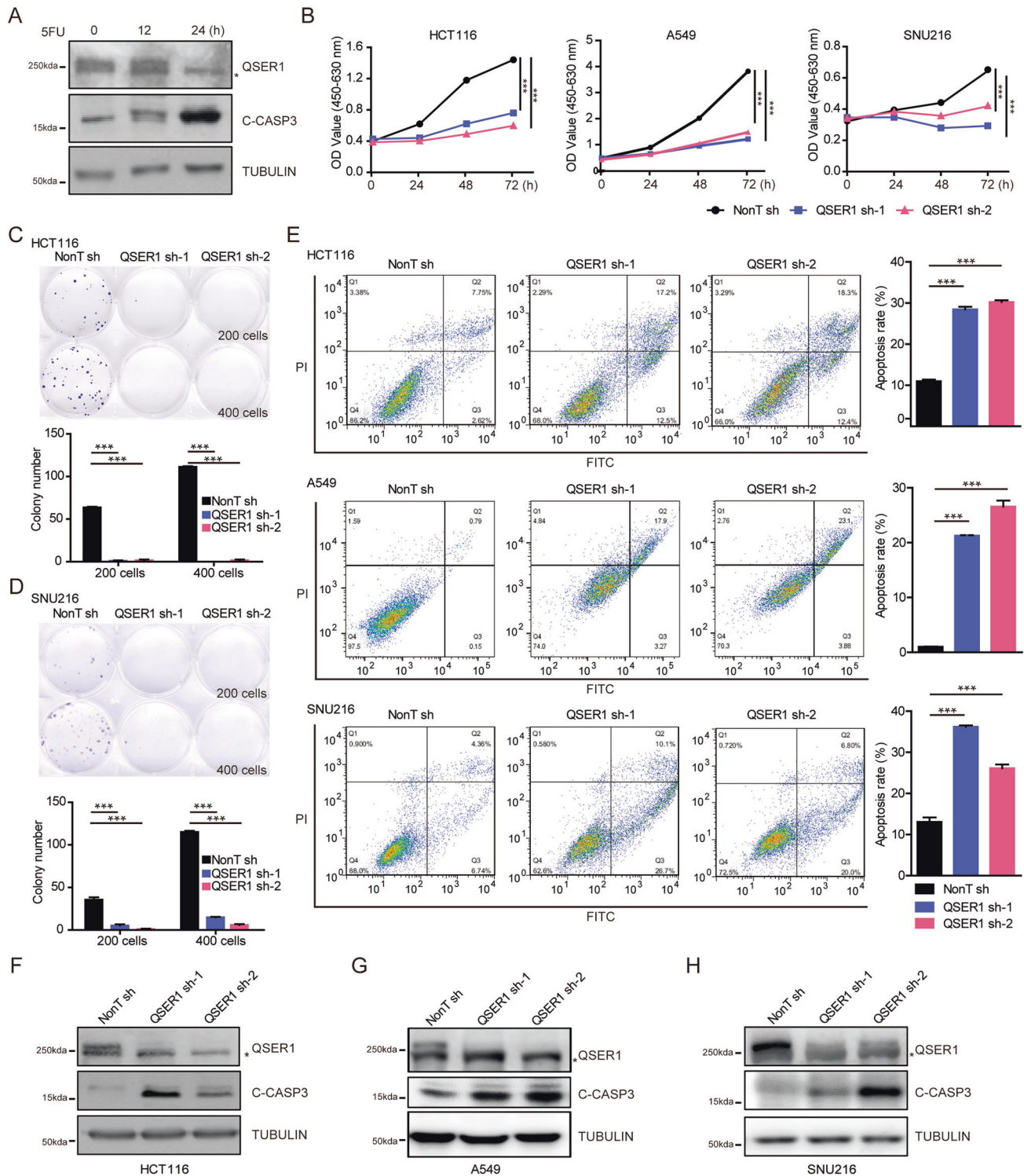
Fig. 2 QSER1 knockdown inhibits cell growth, and induces apoptosis in cancer cells. A Western blot showing the protein levels of QSER1, cleaved-caspase 3 (C-CASP3) in HCT116 cells treated with 350 μM 5-fluorouracil (5-FU) for indicated time. TUBULIN was used as a loading control. *, non-specific band. **B** CCK8 assay show cell viability in control (NonT shRNA) and QSER1 knockdown HCT116, A549, and SNU216 cells. Data are shown as the means ± SEM. ***P < 0.001. Crystal violet staining show colony formation ability of control (NonT shRNA) and QSER1 knockdown HCT116 (**C**) and SNU216 (**D**) cells. Data are shown as the means ± SEM. ***P < 0.001. **E** Flow cytometry analysis detected the proportion of apoptosis in control and QSER1 knockdown in HCT116, A549 and SNU216 cells. Data are shown as the means ± SEM. ***P < 0.001.Western blot showing the protein levels of QSER1 and cleaved-caspase 3 in control and QSER1 knockdown HCT116 (**F**), A549 (**G**), and SNU216 (**H**) cells. TUBULIN was used as a loading control. *, non-specific band.
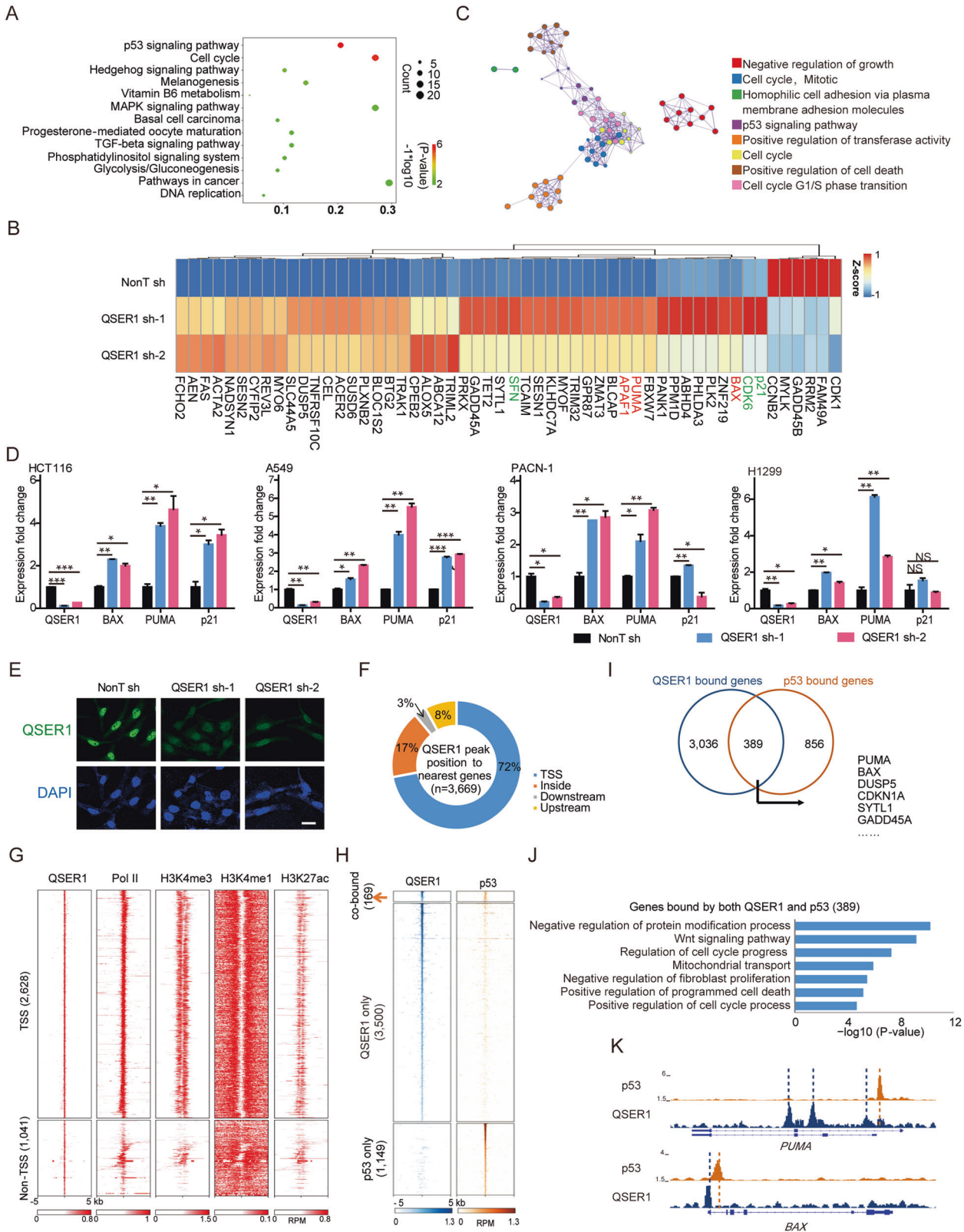
bound by QSER1 (Fig. S4E), including *PUMA*, *BAX*, *BLOC1S2*, and *SYTL1* (Figs. 3B, S4F). To further examine whether and how QSER1 and p53 coordinate to regulate this subset of pro-apoptotic genes, we performed p53 ChIP-seq and identified a total of 1318 p53 bound regions in HCT116 cells. p53 was mainly detected in the

non-TSS regions, where typical p53 recognition motif was highly enriched (Fig. S4G, H). Surprisingly, clustering analyses revealed that less than 5% of the QSER1 bound regions were co-occupied by p53 (Fig. 3H). We then assigned QSER1 and p53 bound peaks to their nearest genes, respectively. Interestingly, 389 genes were

Fig. 3 QSER1 represses p53 target apoptosis genes through binding to these gene loci. A KEGG pathway analysis showing the signaling pathways enriched in the 810 differentially expressed genes after QSER1 knockdown. **B** Heatmaps showing the expression of the 54 known p53 directly activated genes in control and QSER1 knockdown HCT116 cells. **C** Metascape analysis shows part of the network of the signaling pathways enriched in the QSER1-affected genes. The complete network map was shown in Supplementary Fig. 3E. **D** RT-qPCR showing the expression of QSER1, *BAX*, *PUMA*, and *p21* in control and QSER1 knockdown HCT116, A549, PANC-1, and H1299 cells after lentiviral transduction 72 h. Data are shown as the means ± SEM. *$P < 0.05$. **$P < 0.01$. ***$P < 0.001$. **E** Immunofluorescence showing localization of QSER1 in HCT116 cells. Strong QSER1 signal reduction was detected after QSER1 knockdown. DNA was counterstained using DAPI. The scale bar is 30 μm. **F** Pie chart showing the percentage of QSER1 peaks overlapping with a transcription start site (TSS), residing within a gene (inside), or upstream or downstream of the nearest gene. **G** Heatmaps showing the binding profiles of QSER1, Pol II, H3K4me3, H3K4me1, and H3K27ac at the QSER1 enriched regions, which were partitioned into two groups: the TSS group, and the non-TSS group. Shown are ±5 kb of the center of the QSER1 peaks. **H** Heatmaps showing the binding profiles of QSER1 and p53 in the QSER1 and/or p53 bound regions, which were partitioned into three groups: the QSER1 and p53 co-bound group, the QSER1 only group, and the p53 only group. Shown are ±5 kb of the center of the QSER1 peaks. **I** Venn diagram showing the overlap between the QSER1 nearest genes and the p53 nearest genes in HCT116 cells. **J** Gene Ontology (GO) term enrichment analysis of the genes bound by both QSER1 and p53. **K** ChIP-seq genome browser track showing the occupancies of p53 and QSER1 at the *PUMA* and *BAX* loci. The centers of the p53 and QSER1 peaks were highlighted by orange and dark blue dotted lines, respectively.

bound by both QSER1 and p53, mainly including genes involved in cell cycle and apoptosis (Fig. 3I, J). For example, genome browser tracks showed that QSER1 and p53 were localized to different regions within the same genes, such as *PUMA* and *BAX* (Fig. 3K). Thus, our data suggest that QSER1 could directly suppress many of the p53 target pro-apoptotic genes.

QSER1 inhibits p53 genomic binding
To explore the potential mechanism of how QSER1 and p53 coordinate to regulate the same subset of genes, we examined the dependency of p53 on QSER1 at chromatin. We first compared the genome-wide occupancy profiles of p53 in control and QSER1 knockdown cells, and found that p53 occupancies were substantially increased at about half of the p53 bound sites after QSER1 knockdown. In addition, QSER1 knockdown cells lost the remaining half of the initial p53 sites, but gained 2313 new p53 binding sites compared with control cells. The differential p53 peaks in control and QSER1 depleted cells were categorized into three groups: increased (Group **A**), lost (Group **B**), and newly gained (Group **C**) (Fig. 4A–C). Motif analysis showed that the p53 consensus sequence was highly enriched in both Group **A** and **C**, but not Group **B** (Fig. 4A), suggesting that QSER1 knockdown might increase the affinity of p53 to the genomic region bearing p53 consensus sequence.

Many of the known p53 target genes, such as *BAX* and *p21*, were enriched in Group **A** (Figs. 4C, S5A). Increased expression of the known p53 target genes after QSER1 knockdown was accompanied by raised occupancies of p53 at these genes (Fig. 4D). We noticed that p53 peaks in Group **B** were predominantly found in TSS and showed in general weaker signals than those in Group **A** (Fig. 4A, B). Thus, it is likely that QSER1 depletion may predominantly lead to increased p53 signals at the canonical p53 non-TSS sites.

It has been well known that the protein levels of p53 are dynamically regulated in order to achieve specific downstream output [23]. Interestingly, total and chromatin bound p53 protein levels were significantly increased after QSER1 knockdown, while its RNA levels remained largely unchanged (Figs. 4E, S5B–D). Therefore, the increased binding of p53 to chromatin after QSER1 knockdown might be largely caused by the increased level of p53 protein. We speculated that QSER1 might affect stability of p53, and performed cycloheximide chase assay, which indicated that p53 was degraded more slowly after QSER1 knockdown (Fig. 4F). We further examined whether and which post-translational modification (PTM) could be responsible for p53 stability upon QSER1 depletion. Overlapping the total 61 reported p53 upstream kinases (https://www.phosphosite.org) with the 810 QSER1 regulated genes, we found five kinases, including the two p53 Ser315 kinases CDK1 [25] and NEK2 [26], were affected after QSER1 knockdown (Fig. S5E). It has been reported that Ser315 phosphorylation is able to induce p53 degradation and attenuate the DNA binding affinity of p53 [27, 28]. Indeed, QSER1

knockdown significantly reduced phosphorylation of p53 at Ser315 (Fig. 4G). Taken together, our results suggest that depletion of QSER1 might stabilize p53 protein levels and increase the binding of p53 to chromatin.

p53 prevents QSER1 from binding to its target promoters
p53 deficiency confers unfavorable outcome in many cancers [29]. QSER1 overexpression was associated with poor cancer prognosis (Fig. 1E). In line with this finding, we found up-regulation of the QSER1 protein, but not RNA, levels in p53 knockout (KO) HCT116 cells (Figs. 4H, S5F, G). Genome-wide occupancy analyses demonstrated that both numbers and occupancies of QSER1 peaks were also generally increased in the absence of p53 (Figs. 4I, S5H), highlighting the mutual regulation of QSER1 and p53 (Fig. 4J). We also noticed that ChIP-seq read the intensity of QSER1 was substantially increased after p53 KO at the *PUMA* and *BAX* TSS, which was originally occupied by p53 (Fig. S5I). Further genome-wide analyses revealed that, after p53 KO, QSER1 was relocated to part of the regions initially bound by p53, majority of which were TSSs occupied by Pol II and H3K4me3 (Fig. 4K–M), implying that p53 might block the binding of QSER1 to the promoters of these p53 target genes. Taken together, our results suggest that QSER1 and p53 could function antagonistically through mutual regulation.

p53 is not absolutely required for repression of the pro-apoptotic genes by QSER1
p53 acts as a transcription factor to directly activate the transcription of *PUMA* and *BAX* [30, 31], thus promoting apoptosis. When treated with the p53 activator Nutlin 3a, only the p53 WT HCT116 cells, but not the mutated or deficient in PANC-1 and H1299, underwent apoptosis (Fig. S6A). However, as we have shown above, QSER1 knockdown induces apoptosis in both p53 WT and mutant cancer cells. This leads us to hypothesize that QSER1 might generally function in suppressing the pro-apoptotic genes, irrespective of p53 status. To elucidate to what degree QSER1 relies on p53 to regulate the expression of *PUMA* and *BAX*, we further depleted QSER1 in p53 KO HCT116 cells. QSER1 knockdown led to increases in both the RNA and protein levels of PUMA and BAX in p53 KO cells, yet lower than the increases in p53 WT cells (Fig. 5A, B). Consistently, increased apoptosis observed upon QSER1 depletion in p53 KO HCT116 cells was less in degree compared with that in p53 WT HCT116 cells, and similar apoptotic effect induced by QSER1 depletion was also observed in p53 mutated H1299, MKN7, and SNU216 cells (Figs. 5C–E, S6B, S7A, B). We then performed Pol II ChIP analyses in WT and p53 KO cells upon QSER1 depletion and found elevated levels of Pol II at the TSSs of *PUMA* and *BAX* after QSER1 knockdown, further substantiating that QSER1 can directly regulate *PUMA* and *BAX* expression at the transcription levels (Figs. 5F, S7C). Taken together, these results suggest that QSER1 can function in suppressing the expression of pro-apoptotic genes, irrespective of p53 status.

Figure A–M showing p53 ChIP-seq, motif analysis, and QSER1-related data.
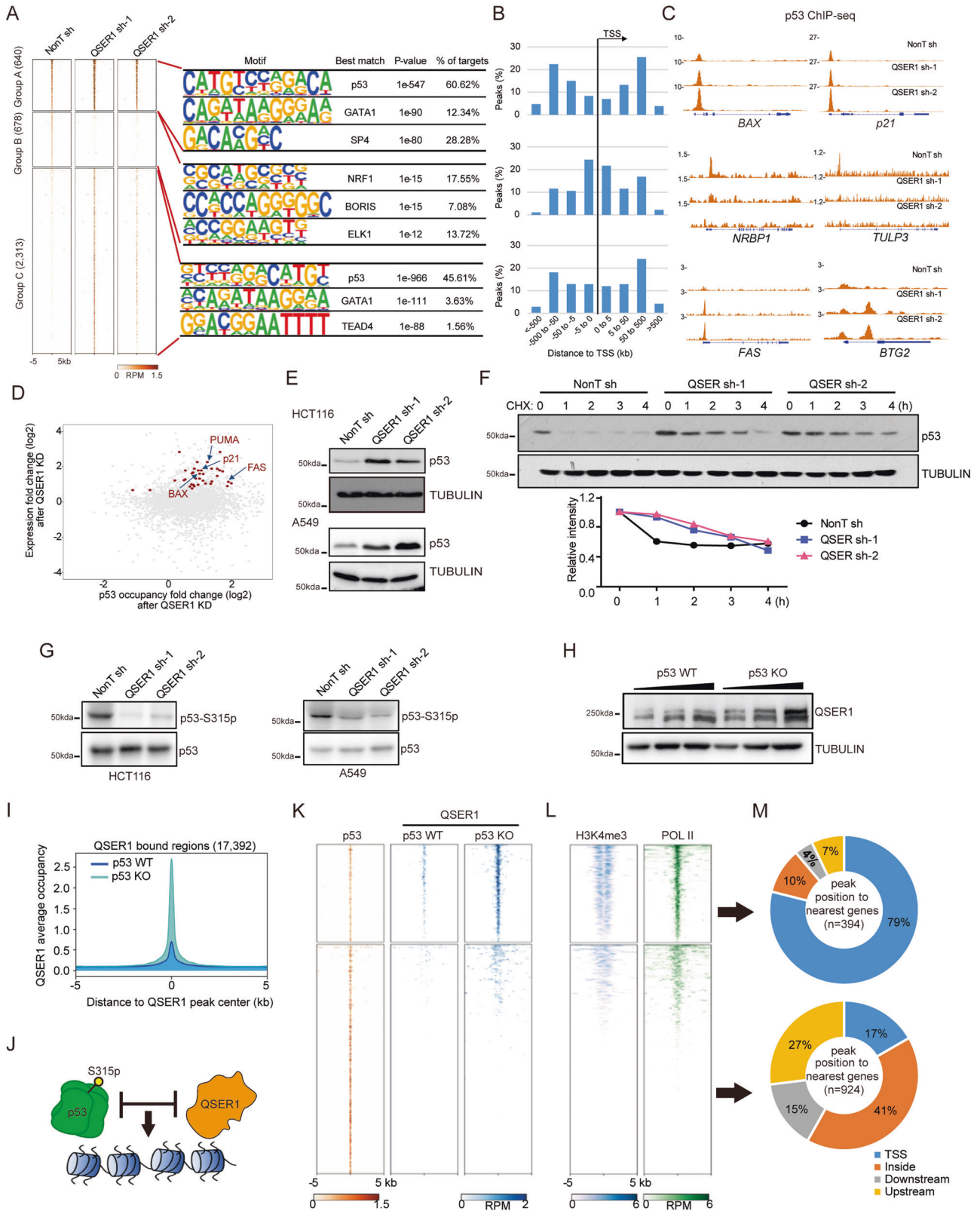
As p53 is frequently mutated in cancers, we examined the expression of QSER1 in p53 mutated clinical cancer samples and found that QSER1 expression was significantly upregulated in many types of cancers carrying p53 mutation compared with p53 WT cancers (Fig. S7D). Interestingly, we also found that *TP53* is ranked as the second frequently altered genes in the 323 QSER1 altered samples out of the 10,960 TCGA pan-cancer samples (Figs. 5G, S7E). Together, our analysis points out a potential role of QSER1 in p53 mutated cancers.

Fig. 4 QSER1 and p53 could function antagonistically through mutual regulation. A Heatmaps (left panel) showing p53 binding profile in control and QSER1 knockdown HCT116 cells. p53 peaks were partitioned into three groups: increased (Group A), lost (Group B), and gained (Group C) groups. Shown are ±5 kb of the center of the p53 peaks. Motif analyses (right panel) of the p53 peaks in the three different groups. **B** Bar graph showing percentage of peak and gene associations according to the distance between p53 peak and its nearest TSS in the three different groups. **C** ChIP-seq genome browser track showing the occupancies of p53 at the representative loci in control and QSER1 knockdown HCT116 cells in the three different groups. **D** Scatterplot correlating gene expression change after QSER1 knockdown (y-axis) versus p53 occupancies change after QSER1 knockdown (x-axis). The known p53 directly activated genes that were up-regulated after QSER1 knockdown were highlighted by dark red dots. **E** Western blot showing the protein levels of p53 in control and QSER1 knockdown HCT116 and A549 cells. TUBULIN was used as a loading control. **F** Western blot showing the protein levels of p53 in control and QSER1 knockdown HCT116 cells treated with cycloheximide (CHX) for indicated time. TUBULIN was used as a loading control. The relative intensity of p53/TUBULIN was qualified using Image J. **G** Western blot showing the protein levels of p53-s315p and p53 in control and QSER1 knockdown HCT116 and A549 cells. **H** Western blot showing the protein levels of p53 in HCT116 WT and p53 KO cells. TUBULIN was used as a loading control. *, non-specific band. **I** Meta plot showing the average QSER1 occupancies in HCT116 WT and p53 KO cells. Shown are ±5 kb of the center of the QSER1 peaks. **J** A schematic showing the mutual regulation of QSER1 and p53. **K** Heatmaps showing the binding profiles of p53 in HCT116 cells, and QSER1 in HCT116 WT and p53 KO cells at the p53 bound regions, which were partitioned into two groups: the QSER1 up-regulated group, and the p53 only group. Shown are ±5 kb of the center of the p53 peaks. **L** Heatmaps showing the binding profiles of H3K4me3 and Pol II in HCT116 cells at the p53 bound regions, which were partitioned into the two groups in **C**. Shown are ±5 kb of the center of the p53 peaks. **M** Pie chart showing the percentage of p53 peaks in the two different groups (**C**) overlapping with TSS, residing within a gene (inside), or upstream or downstream of the nearest gene.

◄—————————————

Deletion of the QSER1 binding site in *PUMA* activates *PUMA* transcription

PUMA is a potent inducer of apoptosis in various cancers [9]. To understand the molecular mechanism underlying the regulation of *PUMA* by QSER1, we interrogated the binding profile of QSER1 over the entire *PUMA* locus. Multiple binding sites of QSER1 were detected within the *PUMA* locus in HCT116 cells. Two of the QSER1 binding regions were located in the TSSs of *PUMA* and *PUMA* antisense RNA, respectively; while the other one, named as the QSER1 binding site in *PUMA* (QBP), was detected in the intron 2 of *PUMA* with strong intensity, which has not been reported previously (Fig. 5H). QSER1 ChIP-seq analyses in HCT116, A549, and HeLa cells revealed that QBP was the only binding site of QSER1 within the *PUMA* locus (Fig. 5H). In addition, the presence of QSER1 on QBP was consistently observed in multiple cancer cell lines (Fig. 5I).

To examine whether QBP is involved in the transcriptional regulation of *PUMA*, we employed CRISPR-mediated genomic deletion to remove QBP from HCT116 cells (Fig. S7F). Two QBP-deleted HCT116 cell lines were obtained (Fig. S7G). Indeed, the expression of *PUMA* was substantially increased in both lines (Fig. 5J). Western blot analyses confirmed that QBP deletion caused the de-repression of PUMA without affecting the protein levels of p53 (Fig. 5K). In addition, we also observed that QBP-deleted cells showed decreases in cell proliferation and clonogenicities when compared with HCT116 WT cells (Figs. 5L, S7H). Intriguingly, the apoptosis rates of these two cell lines were significantly increased after treated with the p53 activator idasanutlin (Fig. 5M), suggesting that the combination of QBP deletion and p53 activator may become a potential cancer treatment strategy. Taken together, our results suggest that QSER1 binds QBP, a novel intronic *cis*-silencing element within *PUMA*, to suppress *PUMA* expression.

QSER1 functions through SIN3A in suppressing *PUMA* expression

To further explore the mechanism underlying the suppression of *PUMA* by QSER1 through QBP, we analyzed published ChIP-seq datasets to identify transcription suppressors that can also bind QBP. We compared the binding profiles of a series of known transcription suppressors, including SIN3A, HDAC1/2, KAP1, SETDB1, and YY1, with QSER1 at the *PUMA* locus (Fig. 6A). Intriguingly, the transcription repressor SIN3A showed similar enrichment profiles with QSER1 within *PUMA* (Fig. 6A), occupying *PUMA* TSS, *PUMA*as TSS and especially QBP. We then examined the occupancies of QSER1 and SIN3A in HCT116 and A549 cells at the genome-wide scale, and found that SIN3A occupied around 80% of QSER1 sites, including QBP and the *BAX* promoter (Figs. 6B, S8A, B). ChIP-qPCR analyses revealed

reduced SIN3A enrichment at the *PUMA* locus in QSER1-depleted cells (Fig. 6C). Co-immunoprecipitation assay showed that QSER1 and SIN3A were able to interact with each other (Fig. 6D). We next examined the effects of SIN3A knockdown on *PUMA* expression, and found that RNA and protein levels of PUMA were substantially up-regulated after SIN3A depletion in p53 WT, KO HCT116 and A549 cells (Figs. 6E, F, S8C). Furthermore, SIN3A knockdown also substantially inhibited cell proliferation, and induced apoptosis in these cell lines (Figs. 6G, S8D). Taken together, our results indicate that QSER1 might generally function together SIN3A to suppress genes such as *PUMA* and induce apoptosis (Fig. 6H).

DISCUSSION

Pro-survival and pro-apoptotic pathways in cancers are sophisticated. An imbalance between them favors cell survival, contributing to cancer progression and chemotherapy resistance [32, 33]. In this study, we demonstrated that QSER1 is a novel anti-apoptotic factor. Our data revealed an essential and general role of QSER1 in anti-apoptosis through repressing the transcription of pro-apoptotic genes (Fig. 7), and suggested that QSER1 inhibition might be a promising therapeutic strategy to induce apoptosis in both p53 WT and mutant cancers.

A general role of QSER1 in apoptosis

It has been well known that activation of the pro-apoptotic genes is essential for inducing apoptosis. The pro-apoptotic genes, especially *PUMA*, are highly regulated at the transcription level. The basal expression level of PUMA is lowly maintained in unstressed cells as the high GC-rich region within intron 1 restricts its promoter's accessibility to the transcriptional machinery [7]. Upon various genotoxic stresses, *PUMA* can be activated by many different transcription factors, including p53, NF-κB [34], c-MYC [35], CHOP [36], E2F1 [37], and members of the p53 family p63 and p73 [38] through the intron 1 regulatory region. However, how *PUMA* and pro-apoptotic genes remain transcriptionally suppressed under normal conditions is largely unexplored. Here, we showed that depletion of QSER1 generally derepresses *PUMA* and *BAX*, and induces apoptosis in various p53 WT, KO, and also mutant cell lines. Intriguingly, scrutinizing its binding profile over the *PUMA* locus, we found that QSER1 is enriched not only at the p53-bound intron 1 region, but also a novel QSER1-specific intronic DNA element, named QBP, across many different cell types. Our data unraveled a novel molecular signaling mediated by QSER1 in inhibiting apoptosis through maintaining the suppressive state of pro-apoptotic genes in a p53-dependent and -independent manner.
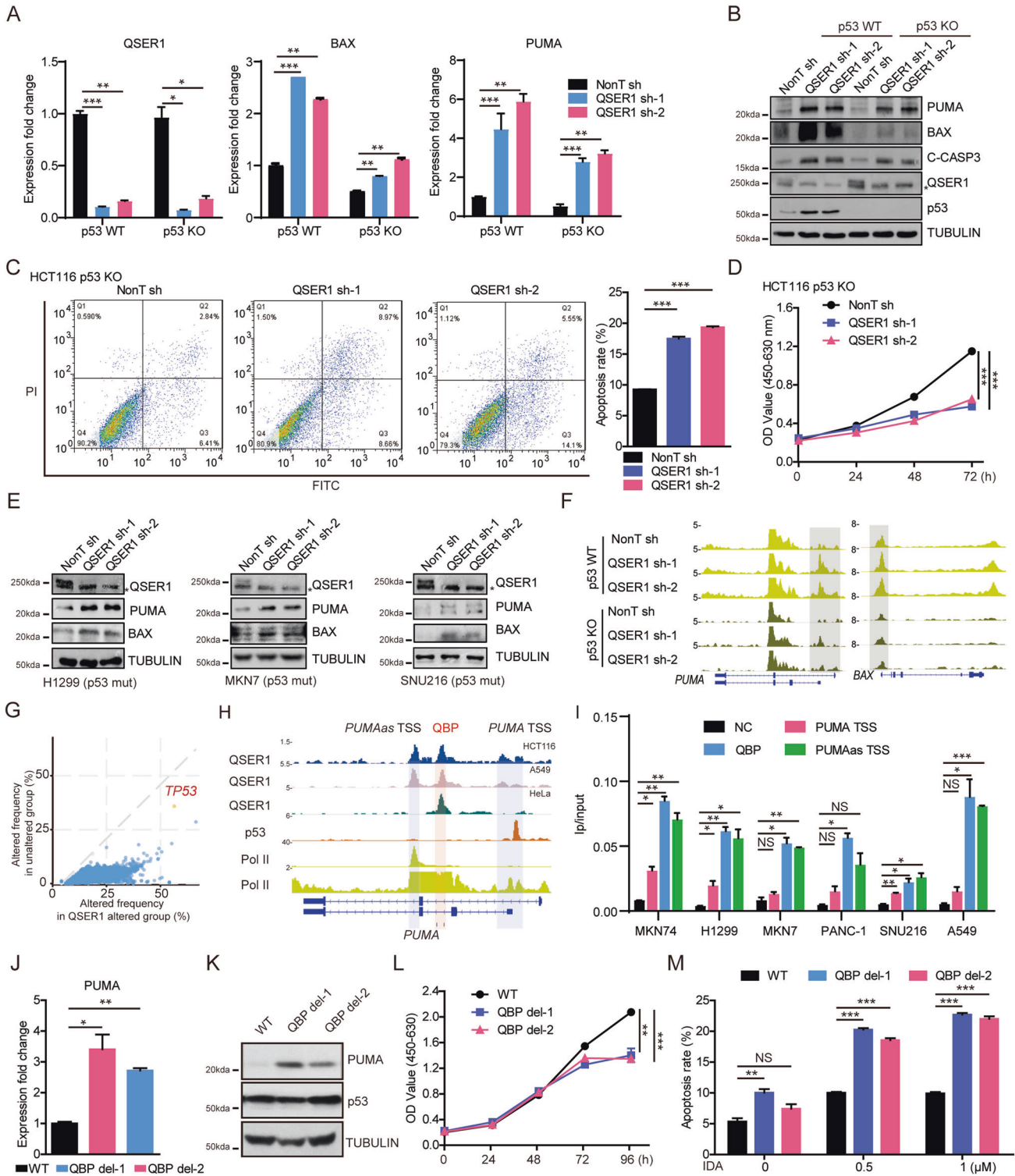
Suppression of the pro-apoptotic genes by QSER1 in a p53-dependent and -independent manner

Many of the QSER1 directly regulated pro-apoptotic genes are also p53 target genes. Here, we for the first time show that QSER1 functions as a multi-faced regulator of p53, and the pro-apoptotic p53-target signaling as well. Interestingly, significant increases in p53 protein levels and chromatin occupancies, largely due to increased protein stability, were observed in QSER1-depleted cells. It is well known that the levels of p53 in cells are tightly regulated via PTM by more than 200 different regulators reported. QSER1 knockdown affected the expression of some of the p53 PTM regulators, including CDK1 and NEK2 that phosphorylate p53 at Ser315. Consistently, we found here that QSER1 knockdown led to a substantial reduction in phosphorylation of Ser315 of p53, which might at least partially stabilize p53 protein. It is worth further investigation that QSER1 may regulate various p53 PTMs under different stress conditions in controlling cell survival.

Fig. 5   QSER1 represses p53 target pro-apoptotic genes in the absence of p53. A RT-qPCR showing the expression of *QSER1*, *PUMA,* and *BAX* in control and QSER1 knockdown HCT116 WT or p53 KO cells. Data are shown as the means ± SEM. *$P < 0.05$. **$P < 0.01$. ***$P < 0.001$. **B** Western blot showing the protein levels of PUMA, BAX, QSER1, cleaved-caspase 3 and p53 in control and QSER1 knockdown HCT116 WT or p53 KO cells. TUBULIN was used as a loading control. *, non-specific band. **C** Flow cytometry analysis detected the proportion of apoptosis in control and QSER1 knockdown in HCT116 p53 KO cells. Data are shown as the means ± SEM. ***$P < 0.001$. **D** CCK8 assay show cell viability in control and QSER1 knockdown HCT116 p53 KO cells. Data are shown as the means ± SEM. ***$P < 0.001$. **E** Western blot showing the protein levels of PUMA, BAX, and QSER1 in control and QSER1 knockdown H1299, MKN7, or SNU216 cells. TUBULIN was used as a loading control. *, non-specific band. **F** ChIP-seq genome browser track showing the occupancies of Pol II at the *PUMA* and *BAX* loci in control and QSER1 knockdown HCT116 WT or p53 KO cells. The *PUMA* and *BAX* TSS regions were highlighted by gray bars. **G** Scatterplot showing the altered frequency of the mutations that correlate with QSER1 mutation and non-mutation group. The *TP53* mutation is marked as orange spot. **H** ChIP-seq genome browser track showing the occupancies of QSER1, p53, and Pol II in *PUMA* TSS, *PUMAas* TSS, and QBP site. **I** ChIP-qPCR showing the enrichment of QSER1 at the indicated regions in MKN74, H1299, MKN7, PANC-1, SNU216, and A549 cells. Data are shown as the means ± SEM. *$P < 0.05$. **$P < 0.01$. NS, no significance. **J** RT-qPCR showing the expression of *PUMA* in WT and QBP deleted HCT116 cells. Data are shown as the means ± SEM. *$P < 0.05$. **$P < 0.01$. **K** Western blot showing the protein levels of PUMA and p53 in WT and QBP deleted HCT116 cells. TUBULIN was used as a loading control. **L** CCK8 assay show cell viability in WT and QBP-deleted HCT116 cells. Data are shown as the means ± SEM. **$P < 0.01$. ***$P < 0.001$. **M** Flow cytometry analysis detected the proportion of apoptosis in WT and QBP-deleted HCT116 cells after treatment with idasanutlin. Data are shown as the means ± SEM. **$P < 0.01$. ***$P < 0.001$. NS, no significance.

We found that as a safeguard for cancer survival signaling, QSER1 can also suppress the pro-apoptotic p53-target signaling in the absence of p53. Most interestingly, QSER1 binds to the pro-apoptotic p53-target loci at previously uncharacterized regions, such as QBP. QBP deletion is able to induce *PUMA* transcription in the absence of genotoxic stress, suggesting that QBP might be an inhibitory element for PUMA to prevent inappropriate activation of apoptosis program under unstressed condition. SIN3A is the central scaffold protein of the SIN3A-HDAC1 corepressor complex [39]. SIN3A has also been found to function with TET1 in activating and repressing gene expression [40]. A recent study reported an interaction of QSER1 with TET1 in protecting bivalent gene promoters and enhancers from hypermethylation [17]. Here we found that QSER1 interacted with SIN3A and depletion of QSER1 disrupted SIN3A occupancies over *PUMA*. It is likely that QSER1 could function through both SIN3A-HDAC and TET1 to maintain a low expression level of *PUMA*, independent of p53. Further investigation into QSER1 regulated cis-elements in other pro-apoptotic genes may provide new functional insight into apoptotic stress control.

The potential clinical application of QSER1 in cancers
QSER1 is significantly upregulated and associated with poor clinical outcomes in many types of cancers, suggesting that QSER1 may serve as a cancer biomarker. A previous report also observed the QSER1 peptides in ovarian cancer patients' plasma [16]. Further studies are needed to investigate whether plasma QSER1 peptide levels can be used for diagnosis or reflect the prognosis of QSER1 up-regulated cancers. In the other hand, the up-regulation of QSER1, irrespective of *TP53* status, could be a strategy of cancer cells developed to escape apoptosis. *TP53* somatic mutations are frequently found in human tumors and are associated with poor patient prognosis. Cancers with *TP53* mutations were hard to be targeted through p53 activators to restore their activity [41]. Thus, further studies are needed to investigate by which mechanisms p53 antagonize the expression or protein stability of QSER1, which may lead to the identification of upstream regulation signaling as an alternative strategy to target QSER1 for cancer therapy.

MATERIALS AND METHODS
Tissue samples and immunohistochemistry
Tissue microarrays were generated using the tissues from 60 pancreatic carcinomas patients by Shanghai Outdo Biotech Company, including tumor and adjacent tissues. Immunohistochemistry (IHC) of QSER1 was carried out using the standard streptavidin-peroxidase (S-P) method. QSER1 immunostaining was assessed independently by two observers (Z.X.R. and H.S.H.). IHC scores were calculated by multiplying an absolute

staining intensity score on a scale of 0–3 (0, negative; 1, weak; 2, mild; and 3, strong) by a positive rate score on a scale of 1–4 (1, positive areas of 0–25%; 2, positive areas of 26–50%; 3, positive areas of 51–75%; and 4, positive areas of 76–100%).

Cell culture
HCT116 WT, HCT116 p53 KO, A549, HEK293T, PANC-1, and HeLa were cultured in DMEM (HyClone) supplemented with 10% FBS (Ex-Cell Bio) and 1% Penicillin–Streptomycin (HyClone). H1299, MKN7, MKN74, and SNU216 were cultured in RPMI 1640 medium (HyClone) supplemented with 10% FBS (Ex-Cell Bio) and 1% Penicillin-Streptomycin (HyClone). All cells were maintained in a humidified incubator at 37 °C under 5% CO_2.

Cell treatment
Cells were treated with 5-fluorouracil (5-FU, sigma F6627), Cycloheximide (CHX, Millipore #239736), Z-VAD(OMe)-FMK (z-VAD, MCE HY-16658), Idasanutlin (IDA, MCE HY-15676) and Nutlin 3a (MCE HY-10029) at indicated concentrations.

Lentivirus mediated RNAi
Human QSER1 shRNA constructs were cloned into the pLKO.1 vector (Addgene). The Non-targeting shRNA construct (SHC002) was purchased from Sigma. Lentiviral particle preparation and infection were performed. Briefly, around 70% confluent HEK293T cells in 150 mm tissue culture plate were co-transfected with 8 μg of the shRNA construct or non-targeting control shRNA, 6 μg of psPAX2 packaging plasmids and 2 μg of pMD2.G envelope plasmids using the Lipofectamine 6000 (Beyotime C0526) or Polyethylenimine branched (sigma #408727). The media were replaced with fresh DMEM supplemented with 10% FBS after 16 h of transfection. The lentiviral supernatants were collected 48 and 72 h after the transfection, filtered through 0.45 μm filters, and concentrated at 18 K rpm for 2 h. Cells were infected with concentrated lentiviral particles with polybrene (Sigma) at the concentration of 8 μg/ml. 24 h after infection, the cells were subjected to selection with 2 μg/ml of puromycin for an additional 48 h.

Annexin V-FITC apoptosis detection
The apoptosis ratio was analyzed using the Annexin V-FITC Apoptosis Detection Kit (Dojindo) according to the manufacturer's instructions. Briefly, $1–5 \times 10^5$ cells were stained with Annexin V and PI for 10 min at room temperature, and immediately analyzed by flow cytometry. Experiments were repeated in triplicate.

Cell cycle detection
For cell cycle detection, cell staining was performed using the Cell Cycle Assay Kit - PI/RNase Staining kit (Dojindo, C543). Concisely, cells were first fixed for 2 h in pre-chilled 70% ethanol at 4 °C. Cells were then stained in the dark for 30 min at 37 °C and finally incubated in the dark for 30 min at 4 °C. Cell cycle was determined by flow cytometry. The results were analyzed using FlowJo 7.6.1 software.
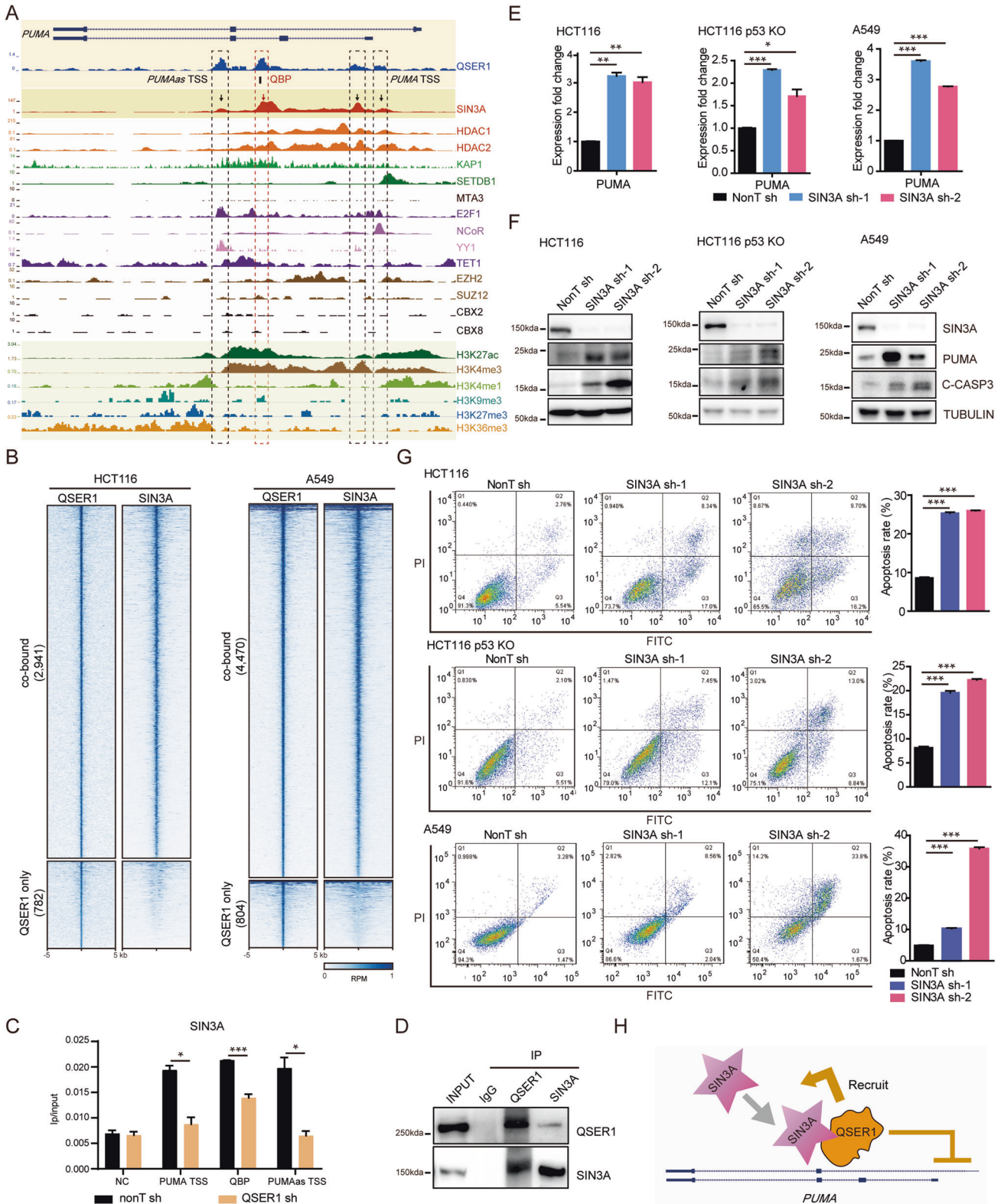
CCK8 assay

Cells were seeded in 96-well plates at 1500 cells/well. 10 μL of CCK-8 (Dojindo) was added to each well at time points of 0, 24, 48, and 72 h of cell growth. Then, after 2 h of incubation at 37 ℃ 5% CO_2, the OD450 and OD630 values were measured using an imaging reader (biotek cytation 5).

Clonogenic assay

The clonogenic assay was performed by seeding 200 or 400 cells/well into six-well plates in triplicate. 11 days after seeding colonies were fixed by 4% formaldehyde and, stained with 0.1% crystal violet dye (Sangon Biotech) dissolved in 2% ethanol, and counted.

Fig. 6 QSER1 functions through SIN3A in suppressing PUMA expression. A ChIP-seq genome browser track showing the occupancies of QSER1, key transcription repressors and histone modifications at the *PUMA* loci. **B** Heatmaps showing the binding profiles of QSER1 and SIN3A co-bound or QSER1 only regions in HCT116 and A549 cells. Shown are ±5 kb of the center of the QSER1 peaks. **C** ChIP-qPCR showing the enrichment of SIN3A at the indicated regions in control and QSER1 knockdown cells. Data are shown as the means ± SEM. *$P < 0.05$. **$P < 0.01$. **D** Endogenous co-IP of QSER1 and SIN3A from HCT116 cells. **E** RT-qPCR showing the expression of *PUMA* in control and SIN3A knockdown in p53 WT or KO HCT116, and A549 cells. Data are shown as the means ± SEM. *$P < 0.05$. ***$P < 0.001$. **F** Western blot showing the protein levels of SIN3A, PUMA, and cleaved-caspase 3 in control and SIN3A knockdown in p53 WT or KO HCT116, and A549 cells. TUBULIN was used as a loading control. **G** Flow cytometry analysis detected the proportion of apoptosis in control and SIN3A knockdown HCT116, HCT116 p53 KO, and A549 cells. Data are shown as the means ± SEM. ***$P < 0.001$. **H** A schematic showing the regulation of QSER1 on *PUMA* by recruiting SIN3A.

Antibodies

The antibodies to PUMA (sc-374223), p53 (sc-126), and p53-s315(sc-135772) were obtained from Santa Cruz. The antibodies to cleaved-caspase 3 (A11021), SIN3A (A1577), and BAX (A0207) were obtained from ABclonal. The antibody to TUBULIN (66031–1) was obtained from Proteintech. The antibodies to Pol II and QSER1 were generated in house.

Chromatin isolation

Cells were incubated in buffer A (10 mM HEPES [pH 7.9], 10 mM KCl, 1.5 mM MgCl$_2$, 0.34 M sucrose, 10% glycerol, Triton X-100 (0.1%), 1 mM DTT, Protease Inhibitor (sigma, P8340) on ice for 5 min. Nuclei were gathered in pellet by low-speed centrifugation (5 min, 1300 × g, 4 °C). Nuclei were washed once with buffer A, then lysed in buffer B (3 mM EDTA, 0.2 mM EGTA, 1 mM DTT, protease inhibitors) on ice for 30 min. Sample was retained by low-speed centrifugation (4 min, 1700 × g, 4 °C). Insoluble chromatin was collected after washing in buffer B and centrifuging under the same conditions.

Immunofluorescence

Cells were grown on coverslips, fixed with 4% paraformaldehyde for 20 min, and blocked with 10% BSA solutions before immunostaining. Primary antibodies were applied in antibody dilution buffer (1 × PBS, 1% BSA, 0.3% Triton X-100) overnight at 4 °C. After three times of washes with PBST, coverslips were incubated at room temperature with secondary antibodies (anti-rabbit IgG Alexa fluor 488, 1:2000) for 1 h, followed by three times of washes with PBST. Cover glasses were mounted on slides in Vectashield containing DAPI and visualized under fluorescent microscope.

Immunoprecipitation

Immunoprecipitation was performed as previously described [42]. Briefly, HCT116 cells were lysed in high salt lysis buffer. After Incubation for 30 min at 4 °C, centrifuge at high speed, remove the supernatant, and add equilibration buffer to bring the final NaCl concentration to 300 mM. Antibody and protein A beads were then added to the samples and incubated overnight at 4 °C. Beads were spun down and washed 3 times with wash buffer before boiling in SDS loading buffer.

Western blot

Proteins were resolved in SDS-PAGE gels and transferred to polyvinylidene fluoride (PVDF) membrane. Primary antibodies used were incubated overnight at 4 °C. HRP-conjugated secondary antibodies (Sigma) were used at a dilution of 1:5000. ECL substrate (Millipore) was applied to the membrane for imaging by autoradiography.

CRISPR-Cas9 guided knockout of QBP

sgRNA oligos targeted the QBP region were cloned into the lentiCRISPR v2 (Addgene). Lentiviral particle preparation was performed as described above. HCT116 cells were infected and selected with puromycin for 48 h. The infected cells were maintained until cell clones were ready to be picked. The clones were screened with PCR, and confirmed by TA cloning and sequencing.

CRISPR-Cas9 mediated knockdown

An inducible lentiviral Cas9 vector (pCW-CAS9; Addgene 50661) was used to generate stable Cas9-expressing HCT116 cells. sgRNAs were cloned into pLKO5.sgRNA.EFS.PAC vector (Addgene 57825). The stable Cas9-expressing HCT116 cells with doxycycline (Sigma) pre-treated 48 h were infected with QSER1 sgRNAs. 6 days after infection, the cells were harvested for further analyses.

Quantitative RT-PCR and RNA-seq library preparation

Total RNA was extracted by using the RNeasy kit (Qiagen) according to the instructions of the manufacturer. RNA was treated with RNase-free DNase I (New England Biolabs), and re-purified on the column. Reverse transcription was performed by PrimeScript™ RT Master Mix (TaKaRa). cDNA was amplified using iTaq™ Universal SYBR® Green Supermix (Bio-Rad) on CFX96 (Bio-Rad). The relative expression levels of genes of interest were normalized to the expression of the housekeeping gene *GAPDH*.

RNA-seq libraries were generated using the VAHTS mRNA-seq v2 Library Prep kit for Illumina (Vazyme) according to the instructions of the manufacturer. Briefly, polyadenylated RNA was fragmented and reversed transcribed. Then the reversed cDNA was ligated to adapters for sequencing.

ChIP and ChIP-seq library preparation

ChIP was performed according to the previously published protocol [43]. Fixed chromatin was sonicated into 200–800 bp fragments (Bioruptor, Diagenode) in ChIP lysis buffer (10 mM Tris-HCl [pH 8.0], 100 mM NaCl, 1 mM EDTA, 0.5 mM EGTA, 0.1% Na-Deoxycholate, 0.5% N-lauroylsarcosine) supplemented with protease inhibitor cocktail (Sigma). Chromatin extracts were incubated with specific antibody and protein A agarose beads at 4 °C overnight. Immunoprecipitates were washed with RIPA buffer (50 mM HEPES-KOH [pKa 7.55], 500 mM LiCl, 1 mM EDTA, 1.0% NP-40, 0.7% Na-Deoxycholate) five times and TE once. After the final wash, DNA was eluted and reverse-crosslinked at 65 °C. DNA was then purified and used as a template for qPCR or for ChIP-seq libaray preparation. Libraries were prepared with NEB Next sample prep kit (NEB) for further next-generation sequencing. For Chip-qPCR, two primers targeting non-regulatory region were used as negative controls (NC).

RNA-seq data processing

The clean reads were aligned to the human genome (hg19) using TopHat (v2.1.0) [44] with default parameters. The Cuffdiff program within Cufflinks (v1.2.0) was used to test statistically significant differences in genes expressions between control and QSER1 knockdown cells [44]. And the expression levels were quantified to fragments per kilobase million (FPKM). Correlation analysis was performed on each RNA-seq data using R software and Corrplot package (https://github.com/taiyun/corrplot).

The differentially expressed genes after QSER1 knockdown were used for Gene Ontology (GO) analysis and gene function clustering network by Metascape [45] (https://metascape.org/). The KEGG pathway analysis was performed using an online tool DAVID [46] (https://david.ncifcrf.gov/home.jsp) and plot was generated by R package ggplot2 [47].

ChIP-seq data processing

The clean reads were aligned to the human genome (hg19) using Bowtie2(v 2.3.5.1) [48] allowing uniquely mapping reads only, and converted to BAM format with Samtools [49]. Peaks were called with Homer (v4.11) [50] ($p < 1e-5$) and the density tracks were normalized to reads per million (RPM) based on mapping results. ChIP-seq data from previously published studies were processed with the same settings

The location of peaks were annotated in terms of genomic features by R package ChIPseeker [51] (tssRegion = c(−500,500)). The cluster analysis was through deeptools(v3.5.1) [52] and bedtools(v2.30.0) [53]. The regions of each cluster were extracted and used for the motif analyses by Homer program findMotifsGenome.pl (-len 8,10,12), and the downstream analysis was performed by GREAT (v4.0.4) [54] (http://great.stanford.edu). The ChIP-seq and RNA-seq data were deposited in the GEO dataset under the accession number GSE180229.
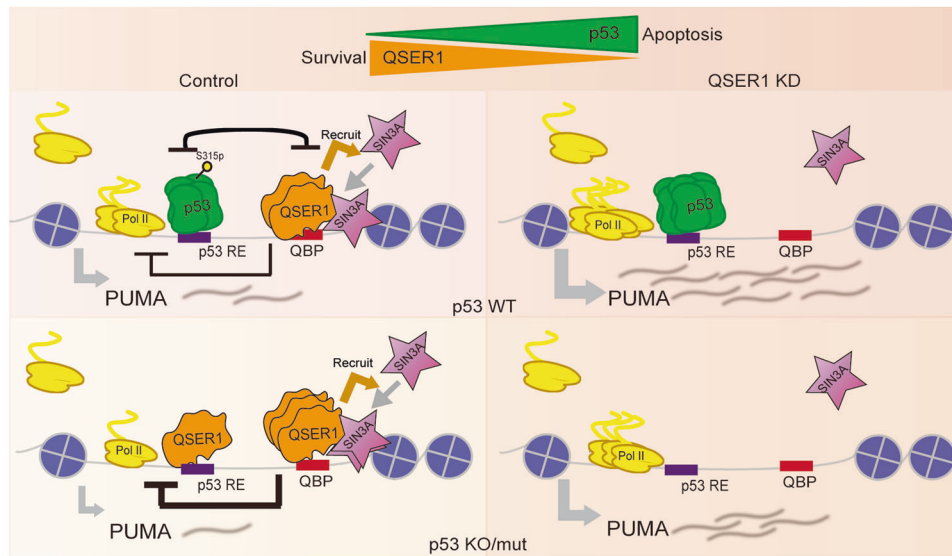
Fig. 7 Working model of QSER1 mediated suppression of the pro-apoptotic genes. QSER1 functions antagonistically with p53 to balance survival and apoptosis (upper panel). QSER1 and p53 occupy distinct regulatory regions of the pro-apoptotic genes, such as *PUMA*, and regulate their expression in the opposite direction (middle left panel). QSER1 functions together with SIN3A to preserve the suppressive status of the pro-apoptotic genes in both p53 WT and deficient cells (middle and lower left panel). QSER1 depletion leads to increases in both protein stability and chromatin occupancy of p53, thus activating the pro-apoptotic genes in p53 WT cancer cells (middle right panel). While in p53 deficient cancer cells, QSER1 depletion also results in de-repression of *PUMA* expression (lower right panel).

ChIP-seq data		
SIN3A	GEO Datasets	GSM935289
SIN3A	GEO Datasets	GSM2423593
SIN3A	GEO Datasets	GSM1010905
p53	GEO Datasets	GSM5369784
HDAC1	GEO Datasets	GSM1003448
HDAC2	GEO Datasets	GSM1003447
KAP1	GEO Datasets	GSM1010849
SETDB1	GEO Datasets	GSM935458
MTA3	GEO Datasets	GSM1010729
E2F1	GEO Datasets	GSM935484
NCoR	GEO Datasets	GSM1003565
YY1	GEO Datasets	GSM803381
TET1	GEO Datasets	GSM5242650
EZH2	GEO Datasets	GSM1003489
SUZ12	GEO Datasets	GSM1003545
CBX2	GEO Datasets	GSM1003567
CBX8	GEO Datasets	GSM1003569
H3K4me3	GEO Datasets	GSM2533929
H3K4me3	GEO Datasets	GSM1003561
H3K4me1	GEO Datasets	GSM2527547
H3K4me1	GEO Datasets	GSM1003453
H3K27ac	GEO Datasets	GSM2534278
H3K27ac	GEO Datasets	GSM1003578
H3K9me3	GEO Datasets	GSM2527565
H3K36me3	GEO Datasets	GSM2527452
H3K27me3	GEO Datasets	GSM2308613

Clinical data analysis
QSER1 expression in multiple human cancers and in p53-mutant and p53-non-mutant were downloaded from ULCAN (http://ualcan.path.uab.edu/). The clinical outcome analysis of QSER1 was performed using KM plotter (https://kmplot.com/analysis/). The analyses of QSER1 mutation and alteration event frequency genes were performed using cBioPortal database (http://www.cbioportal.org/).

Statistical analysis
For analysis of cell experiments, values are the mean ± SEM of $n = 3$ independent experiments. Two-tailed Student's t test was used to determine the significance of differences.

Oligos used in this study:

RT Primer	
PUMA	Forward: GACCTCAACGCACAGTACGAG
	Reverse: AGGAGTCCCATGATGAGATTGT
p53	Forward: CAGCACATGACGGAGGTTGT
	Reverse: TCATCCAAATACTCCACACGC
BAX	Forward: CCCGAGAGGTCTTTTTCCGAG
	Reverse: CCAGCCCATGATGGTTCTGAT
p21	Forward: TGTCCGTCAGAACCCATGC
	Reverse: AAAGTCGAAGTTCCATCGCTC
QSER1	Forward: ACTGGCGGTAACAGTCCATC
	Reverse: ACCCACAGTGGTTGAGGAAG
SIN3A	Forward: GGTGGAGGATGCGCTATCTTA
	Reverse: GGGTGTCGATGCTCTGAGATTT
ChIP Primer	
PUMA **TSS**	Forward: GGAGATCGCCCAGACACC
	Reverse: TCTGTGTACGCATCGCTGG
QBP	Forward: GATGGGGGATGGGAAACCAG
	Reverse: ATGGGCTGTTAACCCTGTGG

PUMAas TSS	Forward: TGCTGACTCACCGGCTATAA
	Reverse: ACTAGGCCGCCGAGGAGT
Bax	Forward: TGCGGGGCAGCGGCCATTTT
	Reverse: TGAGAGCCCCGCTGAACGT
Negative control-1	Forward: GACTGTACTGTTCAGAGGTGTAT
	Reverse: CCTTCCCTACTCCAGTTACAGA
Negative control-2	Forward: ATTTCCCATCAGTATTGTGACCAA
	Reverse: AGAGTTCTCAGCGGGAGTTTAAAA
Sequencing Primer	
QBP	Forward: AATTGCAGCCCACTGTCTCT
	Reverse: GGTTCCCTAAGGCCTACAGC
sgRNA	
QBP sgRNA-1:	GGACACCGATTTCAAGGCCA
QBP sgRNA-2:	GAGTTGACAGTCCTCCCGCT
QSER1 sgRNA-1:	TTTCTATTGCTGAAGGTGGT
QSER1 sgRNA-2:	AGGGCTCCATCCTGGCAGAC
shRNA	
QSER1 shRNA-1:	
Forward: CCGGGCTCCTGTTGATAGTACATTACTCGAGTAATGTACTATCAACAGGAGCTTTTTTG	
Reverse: AATTCAAAAAGCTCCTGTTGATAGTACATTACTCGAGTAATGTACTATCAACAGGAGC	
QSER1 shRNA-2:	
Forward: CCGGAGCACTCCTTACATAGTTATCCTCGAGGATAACTATGTAAGGAGTGCTTTTTTG	
Reverse: AATTCAAAAAGCACTCCTTACATAGTTATCCTCGAGGATAACTATGTAAGGAGTGCT	
SIN3A shRNA-1:	
Forward: CCGGGGTGGAACAGAATCGTTATTTCTCGAGAAATAACGATTCTGTTCCACCTTTTTG	
Reverse: AATTCAAAAAGGTGGAACAGAATCGTTATTTCTCGAGAAATAACGATTCTGTTCCACC	
SIN3A shRNA-2:	
Forward: CCGGGATCAAATCAGAGGACTATATCTCGAGATATAGTCCTCTGATTTGATCTTTTTG	
Reverse: AATTCAAAAAGATCAAATCAGAGGACTATATCTCGAGATATAGTCCTCTGATTTGATC	

Reporting summary

Further information on research design is available in the Nature Research Reporting Summary linked to this article.

DATA AVAILABILITY

The ChIP-seq and RNA-seq data were deposited in the GEO dataset under the accession number GSE180229. This paper does not report original code.

CODE AVAILABILITY

The ChIP-seq and RNA-seq data were deposited in the GEO dataset under the accession number GSE180229. This paper does not report original code.

REFERENCES

1. Fuchs Y, Steller H. Programmed cell death in animal development and disease. Cell 2011;147:742–58.
2. Hanahan D, Weinberg RA. The hallmarks of cancer. Cell 2000;100:57–70.
3. Chen J. The cell-cycle arrest and apoptotic functions of p53 in tumor initiation and progression. Cold Spring Harb Perspect Med. 2016;6:a026104.
4. Fischer M. Census and evaluation of p53 target genes. Oncogene. 2017;36:3943–56.
5. Muller PA, Vousden KH. Mutant p53 in cancer: new functions and therapeutic opportunities. Cancer Cell. 2014;25:304–17.
6. Duffy MJ, Synnott NC, Crown J. Mutant p53 as a target for cancer treatment. Eur J Cancer. 2017;83:258–65.
7. Yu J, Zhang L, Hwang PM, Kinzler KW, Vogelstein B. PUMA induces the rapid apoptosis of colorectal cancer cells. Mol Cell. 2001;7:673–82.
8. Chen L, Willis SN, Wei A, Smith BJ, Fletcher JI, Hinds MG, et al. Differential targeting of prosurvival Bcl-2 proteins by their BH3-only ligands allows complementary apoptotic function. Mol Cell. 2005;17:393–403.
9. Yu J, Zhang L. PUMA, a potent killer with or without p53. Oncogene. 2008;27:S71–83. Suppl 1
10. Yu J, Zhang L. No PUMA, no death: implications for p53-dependent apoptosis. Cancer Cell. 2003;4:248–9.
11. Mullokandov MR, Kholodilov NG, Atkin NB, Burk RD, Johnson AB, Klinger HP. Genomic alterations in cervical carcinoma: losses of chromosome heterozygosity and human papilloma virus tumor status. Cancer Res. 1996;56:197–205.
12. Giampietro PF. 50 years ago in the journal of pediatrics: understanding the molecular basis of 11p13 deletion. J pediatrics. 2021;230:61.
13. Seabra CM, Quental S, Neto AP, Carvalho F, Gonçalves J, Oliveira JP, et al. A novel Alu-mediated microdeletion at 11p13 removes WT1 in a patient with cryptorchidism and azoospermia. Reprod Biomed Online. 2014;29:388–91.
14. Latourelle JC, Pankratz N, Dumitriu A, Wilk JB, Goldwurm S, Pezzoli G, et al. Genomewide association study for onset age in Parkinson disease. BMC Med Genet. 2009;10:98.
15. Barbitoff YA, Serebryakova EA, Nasykhova YA, Predeus AV, Polev DE, Shuvalova AR, et al. Identification of novel candidate markers of type 2 diabetes and obesity in russia by exome sequencing with a limited sample size. Genes. 2018;9.
16. Dufresne J, Bowden P, Thavarajah T, Florentinus-Mefailoski A, Chen ZZ, Tucholska M, et al. The plasma peptides of breast versus ovarian cancer. Clin Proteom. 2019;16:43.
17. Dixon G, Pan H, Yang D, Rosen BP, Jashari T, Verma N, et al. QSER1 protects DNA methylation valleys from de novo methylation. Science. 2021;372.
18. Wang Y, Shen Y, Dai Q, Yang Q, Zhang Y, Wang X, et al. A permissive chromatin state regulated by ZFP281-AFF3 in controlling the imprinted Meg3 polycistron. Nucleic Acids Res. 2017;45:1177–85.
19. Dai Q, Shen Y, Wang Y, Wang X, Francisco JC, Luo Z, et al. Striking a balance: regulation of transposable elements by Zfp281 and Mll2 in mouse embryonic stem cells. Nucleic Acids Res. 2017;45:12301–10.
20. Wang Y, Ma B, Liu X, Gao G, Che Z, Fan M, et al. ZFP281-BRCA2 prevents R-loop accumulation during DNA replication. Nat Commun. 2022;13:3493.
21. Luo Z, Liu X, Xie H, Wang Y, Lin C. ZFP281 recruits MYC to active promoters in regulating transcriptional initiation and elongation. Mol Cell Biol. 2019;39.
22. Chandrashekar DS, Bashel B, Balasubramanya SAH, Creighton CJ, Ponce-Rodriguez I, Chakravarthi B, et al. UALCAN: a portal for facilitating tumor subgroup gene expression and survival analyses. Neoplasia. 2017;19:649–58.
23. Hafner A, Bulyk ML, Jambhekar A, Lahav G. The multiple mechanisms that regulate p53 activity and cell fate. Nat Rev Mol Cell Biol. 2019;20:199–210.
24. Chen L, Liu S, Tao Y. Regulating tumor suppressor genes: post-translational modifications. Signal Transduct Target Ther. 2020;5:90.
25. Kreis NN, Sanhaji M, Kramer A, Sommer K, Rodel F, Strebhardt K, et al. Restoration of the tumor suppressor p53 by downregulating cyclin B1 in human papillomavirus 16/18-infected cancer cells. Oncogene. 2010;29:5591–603.
26. Choi BK, Dayaram T, Parikh N, Wilkins AD, Nagarajan M, Novikov IB, et al. Literature-based automated discovery of tumor suppressor p53 phosphorylation and inhibition by NEK2. Proc Natl Acad Sci USA. 2018;115:10666–71.
27. Li Y, Cui K, Zhang Q, Li X, Lin X, Tang Y, et al. FBXL6 degrades phosphorylated p53 to promote tumor growth. Cell Death Differ. 2021;28:2112–25.
28. Chan C, Thurnherr T, Wang J, Gallart-Palau X, Sze SK, Rozen S, et al. Global rewiring of p53 transcription regulation by the hepatitis B virus X protein. Mol Oncol. 2016;10:1183–95.
29. Bykov VJN, Eriksson SE, Bianchi J, Wiman KG. Targeting mutant p53 for efficient cancer therapy. Nat Rev Cancer. 2018;18:89–102.
30. Chipuk JE, Kuwana T, Bouchier-Hayes L, Droin NM, Newmeyer DD, Schuler M, et al. Direct activation of Bax by p53 mediates mitochondrial membrane permeabilization and apoptosis. Science. 2004;303:1010–4.
31. Dai H, Pang YP, Ramirez-Alvarado M, Kaufmann SH. Evaluation of the BH3-only protein Puma as a direct Bak activator. J Biol Chem. 2014;289:89–99.
32. Johnstone RW, Ruefli AA, Lowe SW. Apoptosis: a link between cancer genetics and chemotherapy. Cell. 2002;108:153–64.
33. Adams JM, Cory S. The Bcl-2 apoptotic switch in cancer development and therapy. Oncogene. 2007;26:1324–37.
34. Bauer A, Villunger A, Labi V, Fischer SF, Strasser A, Wagner H, et al. The NF-kappaB regulator Bcl-3 and the BH3-only proteins Bim and Puma control the death of activated T cells. Proc Natl Acad Sci USA. 2006;103:10979–84.
35. Fernandez PC, Frank SR, Wang L, Schroeder M, Liu S, Greene J, et al. Genomic targets of the human c-Myc protein. Genes Dev. 2003;17:1115–29.

36. Galehdar Z, Swan P, Fuerth B, Callaghan SM, Park DS, Cregan SP. Neuronal apoptosis induced by endoplasmic reticulum stress is regulated by ATF4-CHOP-mediated induction of the Bcl-2 homology 3-only member PUMA. J Neurosci. 2010;30:16938–48.

37. Hershko T, Ginsberg D. Up-regulation of Bcl-2 homology 3 (BH3)-only proteins by E2F1 mediates apoptosis. J Biol Chem. 2004;279:8627–34.

38. Kerr JB, Hutt KJ, Michalak EM, Cook M, Vandenberg CJ, Liew SH, et al. DNA damage-induced primordial follicle oocyte apoptosis and loss of fertility require TAp63-mediated induction of Puma and Noxa. Mol Cell. 2012;48:343–52.

39. Bansal N, David G, Farias E, Waxman S. Emerging roles of epigenetic regulator Sin3 in cancer. Adv Cancer Res. 2016;130:113–35.

40. Zhu F, Zhu Q, Ye D, Zhang Q, Yang Y, Guo X, et al. Sin3a-Tet1 interaction activates gene transcription and is required for embryonic stem cell pluripotency. Nucleic Acids Res. 2018;46:6026–40.

41. Ladds M, Lain S. Small molecule activators of the p53 response. J Mol Cell Biol. 2019;11:245–54.

42. Lin C, Smith ER, Takahashi H, Lai KC, Martin-Brown S, Florens L, et al. AFF4, a component of the ELL/P-TEFb elongation complex and a shared subunit of MLL chimeras, can link transcription elongation to leukemia. Mol Cell. 2010;37:429–37.

43. Guo C, Che Z, Yue J, Xie P, Hao S, Xie W, et al. ENL initiates multivalent phase separation of the super elongation complex (SEC) in controlling rapid transcriptional activation. Sci Adv. 2020;6:eaay4858.

44. Trapnell CRA, Goff L, Pertea G, Kim D, Kelley DR. Differential gene and transcript expression analysis of RNA-seq experiments with TopHat and Cufflinks. Nat Protoc. 2012;7:562–78.

45. Zhou Y, Zhou B, Pache L, Chang M, Chanda SK. Metascape provides a biologist-oriented resource for the analysis of systems-level datasets. Nat Commun. 2019;10.

46. Huang DW, Sherman BT, Lempicki RA. Systematic and integrative analysis of large gene lists using DAVID bioinformatics resources. Nat Protoc. 2009;4:44.

47. Ginestet C. ggplot2: elegant graphics for data analysis. J R Stat Soc. 2011;174:245–6.

48. Langmead B, Salzberg SL. Fast gapped-read alignment with Bowtie 2. Nat Methods. 2012;9:357–9.

49. Li H, Handsaker B, Wysoker A, Fennell T, Ruan J, Homer N, et al. The sequence alignment/map format and SAMtools. Bioinformatics. 2009;25:2078–9.

50. Heinz S, Benner C, Spann N, Bertolino E, Lin YC, Laslo P, et al. Simple combinations of lineage-determining transcription factors prime cis-regulatory elements required for macrophage and B cell identities—ScienceDirect. Mol Cell. 2010;38:576–89.

51. Guangchuang Y, Li-Gen W, Qing-Yu H. ChIPseeker: an R/bioconductor package for ChIP peak annotation, comparison and visualization. Bioinformatics. 2015;31:2382–3.

52. Fidel R, Ryan DP, Björn G, Vivek B, Fabian K, Richter AS, et al. deepTools2: a next generation web server for deep-sequencing data analysis. Nucleic Acids Res. 2016:W160-W5.

53. Quinlan AR, Hall IM, Quinlan AR, Hall IM. BEDTools: a flexible suite of utilities for comparing genomic features. Bioinformatics. 2010;26:841–2.

54. Mclean CY, Bristor D, Hiller M, Clarke SL, Schaar BT, Lowe CB, et al. GREAT improves functional interpretation of cis-regulatory regions. Nat Biotechnol. 2010;28:495–501.

AUTHOR CONTRIBUTIONS
KF, CL, and ZL designed the study, and wrote the manuscript with the assistance of the other authors. XZ, KF, RY, FL, YW, M.F., and SH performed the experiments. XZ, KF, XL, MW, YL, JH, CL, and ZL analyzed the data. CG collected and analyzed the clinical data. WH discussed and wrote the manuscript. CL and ZL provided resources, funding, and supervised the work.

COMPETING INTERESTS
The authors declare no competing interests.

ADDITIONAL INFORMATION
Supplementary information The online version contains supplementary material available at https://doi.org/10.1038/s41418-022-01085-x.

Correspondence and requests for materials should be addressed to Chengqi Lin or Zhuojuan Luo.

Reprints and permission information is available at http://www.nature.com/reprints

Publisher's note Springer Nature remains neutral with regard to jurisdictional claims in published maps and institutional affiliations.